Producing oxygen and fertilizer with the Martian atmosphere by using microwave plasma

Producing oxygen and fertiliser with the Martian atmosphere using microwave plasma

Seán Kelly[a]*, Claudia Verheyen[a,b], Aidan Cowley[c] and Annemie Bogaerts[a]

[a]*Research group PLASMANT, Department of Chemistry, University of Antwerp, Universiteitsplein 1, BE-2610 Antwerp, Belgium*
[b]*Chimie des Interactions Plasma-Surface (ChIPS), CIRMAP, Université de Mons, 23 Place du Parc, 7000 Mons, Belgium*
[c]*European Astronaut Centre, European Space Agency, Linder Höhe, D-51147, Germany*

SUMMARY

The potential of microwave (MW) plasma-based in-situ utilisation of the Martian atmosphere is explored with focus on the novel possibility of fixing N_2, for fertiliser production. Conversion in a simulant plasma (i.e., 96/2/2 % CO_2/N_2/Ar), performed under energy conditions similar to the Mars oxygen in-situ experiment (MOXIE) currently on-board NASA's Perseverance rover, demonstrates that O/O_2 formed through CO_2 dissociation facilitates the fixation of the N_2 fraction via oxidation to NO_x. Promising production rates for O_2, CO and NO_x of 47.0, 76.1 and 1.25 g/h, respectively, are recorded with corresponding energy costs of 0.021, 0.013 and 0.79 kWh/g. Notably, O_2 production rates are ~30 times higher than those demonstrated by MOXIE, while the NO_x production rate represents a ~7% fixation of the N_2 fraction present in the Martian atmosphere. MW plasma-based conversion therefore shows great potential as an in-situ resource utilisation (ISRU) technology on Mars, simultaneously fixing N_2 and producing O_2.

Keywords: plasma; nitrogen fixation on Mars; Mars; In-situ Resource Utilisation; ISRU Mars; Oxygen on Mars; plasma-based gas conversion.

INTRODUCTION

The expansion of in-situ resource utilisation (ISRU) technology [1-8] will be a key enabler for both private and public funded space exploration of planets like Mars. The prohibitive cost of bringing fuel, O_2 and food to Mars greatly motivates exploitation of local resources. ESA's Ariane 5G heavy lift rocket, for instance, has a payload cost of ~10,000 $/kg to reach low Earth Orbit (LEO) [9]. The additional costs of sending each kg from LEO to Mars is estimated at over ten times the initial LEO costs [10], leading to a conservative estimate of 100,000 $/kg. This is further compounded by the ~26-month launch window between the Earth and Mars (i.e., the Hohmann transfer orbit), requiring significantly more resources for both human and two-way robotic missions to the red planet compared to what was needed during the Apollo Lunar missions (taking just over eight days from lift off to splash down). Such staggering costs emphasise the necessity for gaining resources in-situ by bringing the means of production rather than traditional supply-dominated payloads. Leveraging technologies for ISRU by 'living off the land' is therefore a central tenet for future space enterprises, with hopes to efficiently utilise locally available renewable electricity, such as solar, to harvest

**E-mail address:* sean.kelly@uantwerpen.be, lead contact

and process native resources. The ISRU paradigm therefore opens many new possibilities for future space exploration [11,12].

In 2021 the National Aeronautics and Space Administration's (NASA) Martian rover 'Perseverance' performed the 'Mars O_2 in-situ resource utilisation experiment' (MOXIE) [13], producing for the first time, extra-terrestrial O_2 using solar-harvested electricity. This milestone event is set to expand innovation in technologies to harvest Martian resources for fuel, life support and materials over the coming decades. The solid oxide electrolysis cell (SOXE) component of the MOXIE experiment demonstrated the production of ~ 6g of O_2 from compressed Martian ambient [14,15] using a full sol energy allocation of 1 kWh (further details are given in the **supplemental information** (**figure S1**)). Human consumption of O_2 is about 1 kg/day [16,17], while utilisation of O_2 in a fuel mixture (e.g., Methalox) to power a Mars Ascent Vehicle (MAV) could require thousands of tonnes of fuel [14,18,19]. Clearly, significant scale-up is required to achieve the aspirations of future ISRU based missions. MOXIE is based on solid oxide electrolysis cell technology and due to the long start-up requirements (~2 hours), the technique is largely inflexible to fluctuating energy production and so requires battery storage from any local renewable energy harvested on Mars. Techniques such as plasma-based gas conversion [20,21], which can match production with the availability of renewable electricity (i.e., fast start-up time), would therefore hold great potential for ISRU applications on the red planet.

Mars, with an atmosphere of ~96% CO_2, ~2 % N_2 and ~2 % Ar [22,23], provides quite favourable low pressure (~1 % of the Earth atmosphere) and temperature (~0 °C to < -60 °C) conditions [22,23] for efficient plasma conversion compared to Earth bound climes. To date, however, the potential for this enticing technology remains largely unexplored in an ISRU context [24-31]. Plasma-based O_2 generation and membrane extraction has previously been proposed using direct current (DC) plasma by *Wu et al.*[24]. *Gruenwald et al*. [25,26] envisaged the use of plasma technology by early Martian settlers for a wide range of applications including O_2 production. More recent reports by *Guerra et al.* [27,28] have demonstrated, again, the potential of DC plasmas under Martian conditions, reiterating the benefits of using the ambient conditions for O_2 production. *Premathilake et al.* reported on the use of a DC plasma generated in-situ of a thin silver membrane which enabled partial oxygen removal [29]. *Moses et al.* [30] uniquely suggested the harvesting of plasma-produced O_2 during the landing descendent to Mars, where solid oxide cell technology could be incorporated into the heat shield to capture O_2. The potential use of microwave (MW) plasma under Martian conditions was recently explored in the PEOMA ('Plasma Extraction of O_2 from Mars Atmosphere') project by *Wheeler et al.*, supported by NASA [31]. Their experimental study, which focused on O_2 production, showed the feasibility for high levels of CO_2 conversion under low Martian pressure (i.e., with low gas flow rate). The energy efficiencies reported via conference proceedings [31] were, however, quite low (i.e., < 10 %). This contradicts previous studies of CO_2 plasma conversion at low pressures (i.e., close or below Martian ambient conditions), which claimed both high efficiency and high conversion levels, even up to 90% at supersonic flow conditions, as reported in the 1980's [32] although the latter findings have not been reproduced to date [33-35]. The proposal for N_2 fixation (NF) with the Martian atmosphere using plasma, has, to the best of our knowledge, not been previously interrogated. This intriguing prospect will therefore be of particular focus in this work.

Artificial N_2 fixation is a cornerstone of modern civilisation and currently sustains over 40 % of Earth's population [36,37]. N is a rate-limiting nutrient for plant growth and is notably absent from the Martian regolith, unlike the other key macronutrients for plant growth, such as K and P, which have been discovered by soil sampling [38-43]. Recent botanical experiments using Martian regolith simulants [38,41] have highlighted that seed germination and plant growth may be possible in controlled environments, such as an underground greenhouse. Future utilisation of Martian regolith as a farming substrate will therefore require production of

N_2-based fertiliser as a key enabler for plant growth to sustain future habitats [7,38,41,44]. Another important potential use for NF on Mars is the production of explosives with potential use for excavations and active seismology studies [45,46].

On Earth, industrial-scale NF is at present achieved via the Haber-Bosch (H-B) process (producing ammonia) in combination with the Ostwald process (converting ammonia to nitric acid) [47]. This energy-intensive process, fueled by natural gas (i.e., methane), has dominated artificial fertiliser production for almost a century and has enabled crop yield enhancements, which at present nourish a large proportion of the world population [48]. Owing to the exceptional stability of the N_2 triple bond, the H-B process is an energy-intensive chemical process, which accounts for ~2 % of the world's energy consumption, consumes ~3 % of the global natural gas output and as a result emits more than 300 million tonnes of CO_2 annually [48]. Recently, efforts to find alternatives to the H-B process, which are not reliant on fossil fuels, have expanded, including significant interest in plasma technology [20,36,37,49].

The large-scale use of plasmas to fix N_2 on Earth for fertiliser production goes back to the Birkeland-Eyde (B-E) process to produce nitric acid and was first developed in the early twentieth century [50-52]. The B-E process converted air to NO_x in an electric arc formed inside an electromagnet followed by an oxidation stage where the remaining NO was converted to NO_2 in settling tanks (i.e., a relatively slow reaction preferable at reduced temperatures). This stage was followed by NO_2 hydrolysis in large water absorption towers packed with quartz segments, eventually producing a solution of HNO_3. The industrialised B-E process produced ~2 % NO_x with an energy consumption for the NO_x plasma synthesis stage of 2.4–3.1 MJ/mol. The absorption stages added approximately 30-40 % additional energy overhead [47,48,51].

A revival of research interest in plasma-based N_2 fixation (i.e., a 21st century B-E process) has occurred recently with the expanding availability of renewable electricity and intense efforts to mitigate anthropogenic climate change [48,53]. Recently [36], we showed very promising metrics for plasma NO_x production and energy cost (under Earth conditions), reaching 3.8 % total NO_x concentration, at a production rate of 0.77 L/min for ~2 MJ/mol energy cost, using atmospheric pressure MW plasmas. To our knowledge, this is the lowest energy cost reported in literature for atmospheric pressure plasmas, at significant NO_x concentrations. Note that we incorporated modern advancements in MW technology, employing a solid-state amplifier, to power the reactor. Of course, such contemporary technology (and indeed MW technology) was not available during the B-E process development in the early twentieth century [54]. Further, solid-state technology can significantly reduce the size and mass associated with MW-powered plasma generation and is therefore much more suitable to meeting the constraints of space deployment [55]. Solid-state power supplies are not only more compact but due to superior control (i.e., over frequency and power) enable compact plasma reactors with the need for 'bulky' waveguide components reduced (e.g., plasma lighting applications [56]). A magnetron-based plasma reactor with a volume of ~25 L and mass ~50 kg (say) could be reduced to 5 L and 5 kg [57].

Microwave (MW) generated plasmas offer desirable characteristics [58] of high ionisation fraction (i.e., electron density) coupled with relatively low mean electron energies. The electric field generated by the applied MW power selectively heats the electrons, due to their small mass. Furthermore, the electron energy of 1-3 eV, combined with high electron density, gives rise to efficient vibrational and electronic excitation, which can in turn significantly promote efficient (i.e., non-thermal) dissociation routes in gases such as N_2 [53]. Along with CO_2 conversion to O_2 and CO, the potential of plasma-based NF by oxidation of the N_2 content (2 %) available in the Martian ambient provides a potential avenue for NF, which has to date not been explored. Vibrational

and electronic excitation of the N_2 fraction in the Martian atmosphere can lower the threshold for breaking the extremely stable N_2 triple bond (~9.8 eV), which can then be oxidised by O/O_2 formed upon conversion of the large amounts of CO_2 present in the Martian atmosphere.

MW plasma technology offers a very high overall power transmission efficiency compared to low-frequency plasma reactor designs [21]. In low-frequency plasma reactors, much of the electrical power can be lost in resistors and reflections due to impedance mismatching (dissipating as heat or nuisance radiation). Even DC-powered plasmas typically have an alternating voltage and current response (due to the RC characteristics of the dynamic plasma and its circuit interaction). Previous studies on plasma-based gas conversion only considered the absorbed plasma power [21] when calculating the energy cost of conversion, which disregards a very large fraction of the real power wasted through transmission to the plasma (e.g., losses can be > 50 % of the overall system power for poorly matched designs, using high resistance components to ballast plasma instabilities), but for practical applications, the input power should be considered, thus accounting also for the transmission efficiency of the power supply. MW plasma using solid state technology can now sustain transmission efficiencies of > 70 % with x10 longer lifetimes compared to magnetron technologies, which degrade in performance comparatively quickly over time. The electromagnetic shielding of high-frequency MW discharges is also much more straightforward compared to low-frequency plasma devices, which present a considerable challenge in terms of minimising electromagnetic interference (EMI) to neighboring electronics (e.g., EMI from arc welders operating at DC and kHz AC are a common nuisance [59,60]). We, therefore, believe that MW plasma generated using state-of-the-art low mass, small footprint solid-state amplifiers is the 'technology of choice' for future missions deploying plasma-based gas conversion technologies to Mars and beyond.

In this work, we explore the feasibility of NF on Mars by in-situ leveraging the indigenous atmosphere in combination with the co-conversion of CO_2 to CO and O_2, for generating resources for fertilisers, fuels and life support systems by means of experiments, benchmarked against MOXIE operating conditions, and supported by chemical kinetics modelling to reveal the underlying mechanism.

RESULTS AND DISCUSSION

The aim of this investigation is to highlight the potential of MW plasma technology for ISRU on Mars. In particular, besides CO_2 conversion into CO and O_2, we also show the novel possibility for N_2 fixation, the most energy-intensive aspect of fertiliser production and therefore, a key requirement for nourishing any potential future Martian settlers. In the first section, we present the results for our MW plasma experiments using a Martian atmosphere mixture, while in the second section we use our corresponding numerical modelling to reveal the underlying mechanisms. This is followed by a discussion outlining possible utilisation scenarios for plasma-based ISRU on Mars. Finally, a conclusion is given.

MW plasma-based conversion in a Martian atmosphere

The operating conditions for our MW plasma reactor are inspired by the current MOXIE experiment on board NASA's Perseverance rover [14]. MOXIE operates with an energy allocation of 1 kWh using a full sol worth of solar harvested electricity. The solid oxide cell apparatus (known as SOXE), which performs the dissociation and purification, specifies an operating pressure ranging from 260 to 760 Torr (or 0.34-1 bar). The lower range of 0.34 bar is incorporated here for our plasma operating conditions. In our setup a vacuum system is employed to lower the pressure inside the reactor to ~0.34 bar, while using a typical swirling mass flow rate

of 10 L/min required to operate the reactor [36]. MOXIE uses lower mass flow rates, given the operation conditions of the Martian atmosphere, where gases are compressed from the ambient conditions (~0.01 bar) to a higher pressure (i.e., 0.34-1 bar) inside the SOXE compartment. In spite of such differences, the key parameters of pressure and power are comparable in both cases and thus our investigation serves to gain insight into conversion rates and energy cost possible using plasma-based gas conversion technology under rover energy conditions.

In the **supplemental information figure S1**, we show graphical results of the historic MOXIE experiment for O_2 production completed during April 2021 [15]. MOXIE operating at a power of 300 W [14] over 3.3 hrs of operation (i.e., ~12000 s) produced 5.4 g of O_2. This encompassed a two-hour warm-up period, followed by ~1 hour of O_2 generation. This yields an O_2 production rate of ~1.6 g/h at an energy cost of 0.19 kWh/g. The overall O_2 produced (i.e., 5.4 g) during the test on April 20th (Sol 70 of the Martian year) used the 1 kWh energy allocation available to MOXIE from solar electricity harvested by panels on the Perseverance rover. Note that MOXIE operates at 300 W, while our MW plasma operated at 1 kW. However, we compare the two processes in terms of energy usage rather than power. Indeed, the MOXIE results from April 2021 (used here as a benchmark) consumed ~1 kWh of solar energy which was applied at a rate of 300 W for ~12000 s (~3.33 h). In comparison, our plasma operates at an energy deposition rate of 1 kW which should run for 1 hr to use the same 1 kWh energy as MOXIE. Since our comparison of production rates is made based on the energy required per gram of CO, O_2 and NO_x produced (i.e., kWh/g) the disparate operating powers are not of particular concern.

In **figure 1 A** we present the production rates of CO, O_2 and NO_x (i.e., sum of NO and NO_2) measured in the plasma exhaust for an inlet mass flow rate of 10 L/min (i.e., 1.131 kg/h CO_2, 30 g/h N_2 and 21.4 g/h Ar mass flow rate for a Martian mixture in a ratio 96/2/2%), at (absorbed) plasma power of 1 kW. We measured a production rate for O_2 of 47.0 $\pm$ 3.9 g/h, while the production rate for CO was found as 76.1 $\pm$ 4.7 g/h. The conversion of CO_2 was measured to be 9.4 $\pm$ 0.4 %, with corresponding yields for O_2 and CO measured as 5.2 $\pm$ 0.2 % and 9.7 $\pm$ 0.6 %, hence the latter approximately two times the O_2 value, which is in-line with the stoichiometry of CO_2 splitting. Notably, the production rates, conversion and product yields were adjusted for the gas expansion, which was measured as ~5% increase of the inlet mass flow (i.e., $\alpha = 1.05$), see **equation 4** in the **Experimental Procedures section**.

From **figure 1 B** we observe that the corresponding energy cost for production of CO and O_2 is 0.0129 $\pm$ 0.0008 and 0.021 $\pm$ 0.002 kWh/g, respectively. Hence, the plasma produces O_2 at an energy cost about an order of magnitude smaller than in the recent MOXIE test, which reported 0.19 kWh/g (see **supplemental information figure S1**), and the O_2 production rate (47.0 g/h) is even ~30 times higher than in the MOXIE test (i.e., ~1.6 g/h). Plasma-based ISRU therefore shows much promise when compared to solid oxygen electrolysis cell (SOEC) production under comparable energy conditions. Note however that the energy gains demonstrated here do not account for the considerable cost of gas compression and separation, along with the energy losses of the solid-state MW power supply employed in this study, which has an efficiency of ~50 % [61]). The energy cost of compressing the Martian atmosphere by the MOXIE experiment, carried out using a scroll pump, is approximately one third of the total energy cost (i.e., ~0.06 kWh/g) [14]. The energy cost of separation is more difficult to estimate, but using the heat available in the plasma exhaust ($T_{exhaust}$ > 1000 K, see discussion below) will be key. Utilisation of this energy could enable the use of O_2 separation technologies, which operate at high temperature. This includes emerging technologies such as oxygen transport membranes [62], or indeed more mature techniques such as solid oxide electrolysis cells. Hence,

synergies with such oxygen separation technologies, enabling production of a pure O_2 stream, and plasma technology may yield very interesting pathways for future innovations. The findings presented here therefore strive to highlight and inspire further interrogation of this potential.

Figure 1 A also shows that the total NO_x production rate was found to be ~1.25 g/h, with an equivalent concentration in the exhaust mixture of 1320 ± 105 ppm (or 0.13 %). NO and NO_2 are the primary species produced with a ratio NO/NO_2 of ~3.4. Notably, no other N_xO_y species (e.g., N_2O) were detected in measurable quantities. This produced NO_x concentration corresponds to ~7% of the N_2 inflow being fixed. The corresponding energy cost for NO_x production is ~0.79 kWh/g, see **figure 1 B**. This is considerably higher than the energy cost of O_2 production, which is like expected given the low fraction of N_2 available in the Martian atmosphere, but at least it serves to give insight into what is possible using plasma-based N_2 fixation on Mars using plasma technology. On Earth, the Haber-Bosch (HB) process fixes about 171 teragram (Tg) of N_2 per year, of which 70 % is used for fertilisers (i.e., 84.7 Tg) [63]. The utilisation of this fixed N_2 (albeit very inefficiently [64,65]) supports at least ~2.8 billion people (i.e., ~40 % of the current world population of 7.2 billion) for their food production. The needs of a Martian settler estimated on this (Earth) basis would be ~3 kg N/yr. or 8.2 g/day, and based on the energy cost of 0.79 kWh/g for NO_x production shown in **figure 1**, this amounts to ~6.5 kWh/day or ~2.36 MWh/yr. of energy expenditure. The cost of producing the ~1 kg of O_2 required daily per person [16], needed to sustain life support on Mars, can be similarly estimated as ~20 kWh/day or ~7.3 MWh/yr. using the energy cost of ~0.02 kWh/g for O_2, presented in **figure 1**. The average daily energy needs for an Earth citizen today are about ~58 kWh [66] with at least 1 % of global energy used for production of nitrogen-based fertilizer (i.e., ~0.58 kWh) [67]. Future Martian settlers will have much greater energy needs compared to their Earth neighbours. Based on our estimates, as detailed above (i.e., ~6.5 kWh/day for NO_x (fertilizer) production and ~20 kWh/day for O_2 production (life support)), nitrogen fertilizers and O_2 alone will require ~27 kWh/day, i.e., almost half the total average Earth residents use today (around 58 kWh, see above).

We measured the exhaust temperature from the plasma using a k-type thermocouple positioned at ~10 cm outside the plasma and afterglow region (i.e., inside the gas connector shown in **figure 3 B** on the right-hand side). We recorded a steady state temperature of ~782 °C (or ~1055 K) for 1 kW absorbed MW power. Note, our gas analysis is performed after the plasma reactor is in operation for at least 15 minutes, after which time the exhausted gas temperature has stabilised, indicating the reactor has reached a steady state operation, although production rates of CO, O_2 and NO_x stabilise much faster (~10 s) compared to temperature. Utilisation of this heat downstream presents an opportunity to reduce overall energy costs, when this energy could be efficiently recovered [68], for example, to heat the incoming gas before plasma conversion (with benefits to CO_2 and N_2 dissociation) or to provide heat energy for another chemical reaction or system downstream. In addition, we plan to explore synergies with O_2 separation technologies which operate at high temperatures, such as SOEC [8,14,69] or oxygen transport membranes [62], by using the heated plasma exhaust to activate a downstream product separation.

Numerical modelling

We applied our chemical kinetics model to our experimental conditions presented in previous section, and **figure 2 A** presents the calculated CO and O_2 concentrations as a function of position in (and after) the plasma region. The measured concentrations (downstream, hence after the plasma) are indicated with stars, for comparison. An O_2 concentration of 6.2 % is predicted at ~35 cm, 15 cm outside the plasma region, which extends from 0 to 20 cm. This compares reasonably well to the value of 5.2 ± 0.5 % measured in our experiment (see star in **figure 2**). The CO concentration predicted by our model is approximately twice the

O_2 concentration, with a value of 12.5 % at ~35 cm, as shown in **figure 2**. This value also compares reasonably to our experimental measurement of 9.7 ± 0.9 %.

Because of this reasonable agreement between model and experiments, we can use the model to analyse the dominant CO and O_2 production reactions. Averaged across the simulation domain, both CO and O_2 are primarily formed via **reaction 13,** involving the collision of O atoms with CO_2, yielding CO and O_2. Our analysis reveals that 85 % of the CO and O_2 produced via **reaction 13** involves the symmetric stretch and bending vibrational modes of CO_2, namely $CO_2(V_a\text{-}V_d)$ (ranging 0.08-0.33 eV in energy) [70], while 8 % occurs from ground state CO_2 and 7 % originates from $CO_2(V_{1\text{-}21})$. This behaviour is generally in agreement with previous reports on CO_2 conversion under similar (warm plasma) conditions [58,71-73]. Note that our model of course depends on input data, such as chemical reactions and corresponding rate coefficients and cross sections, but as this dominant CO_2 conversion mechanism is in agreement with literature, we believe our assumed chemistry is reliable. Other model assumptions and input data in the model, such as mass flow rate, pressure, reactor dimensions, and power density are matched to our experiments as closely as possible. For instance, the power density is determined by the plasma power divided by the plasma volume, both obtained from the experiment, and radial variations are incorporated to represent gas intersecting different regions of the plasma filament, as in our previous work [36]. The asymmetric stretch mode gives rise to the most efficient CO_2 dissociation pathway through a ladder climbing mechanism. However, we see that this mode is relatively supressed here (i.e., ~7 % contribution) due to the relatively high pressures and temperatures under study (0.34 bar, and 2000-3000 K in the plasma filament), which serve to strongly depopulate $CO_2(V)$ via VT relaxation. Lower pressure conditions would allow a much larger contribution of the asymmetric stretch mode, which due to its vibrationally higher energy can significantly reduce the energy cost for dissociation and thus provide improved efficiency. Pressure and temperature conditions more resemblant to the Martian ambient (i.e., ~0.01 bar, -60 C) should, therefore, serve to further increase the promising metrics discovered here. Since compressing the gas has an energy cost, it would be interesting to understand the influence of lower pressures on the results. Typically, plasma-based CO_2 conversion and N_2 fixation are more energy-efficient at lower pressures, because of more pronounced vibrational-translational non-equilibrium, i.e., the vibrational levels of CO_2 and N_2, which give rise to the most efficient conversion [20,21], are more overpopulated at lower pressure, because of reduced losses upon collisions with the ground state molecules. Our preliminary calculation results indeed confirm this better performance at lower pressure, but these results could not yet be compared with experiments, and are thus somewhat speculative. In our future work, we will investigate the effect of Martian pressures on the performance of both CO_2 conversion and N_2 fixation.

Figure 2 B shows our model predicts a steady state total NO_x concentration of ~311 ppm outside the plasma region, at x ~35 cm. Comparatively, the total NO_x concentration in our experiment is measured as ~1320 ppm, hence our model clearly underestimates the NO_x production. *Ramakers et al.* [74] studied a CO_2/N_2 gliding arc plasma under similar conditions, and for the lowest N_2 fraction investigated (5%), they reported a NO_x concentration of about 1500 ppm, hence very similar to our results. In addition, they also showed some discrepancy in absolute values between the simulated and measured NO_x concentration, but the trend as a function of N_2 fraction was correctly captured by the model. We believe the discrepancy in absolute values is attributed to the low N_2 levels simulated, the complexity of the underlying chemistry (which relies on thousands of empirical reaction rate data) and also the inherent physical assumptions required in quasi-1D models of this kind. In spite of this, we believe we can use the model to gain valuable insight into the underlying mechanisms.

We analysed the dominant NO production reactions, given its importance as the key NO_x species (i.e.,

measured NO/NO_2 ratio of ~3.4, and NO is precursor for NO_2, see **reaction 11**). The Zeldovich reaction between N_2 and O atoms (**reaction 9**) is found to contribute for 51 % to the overall NO formation. This involves a contribution of 42.5% from electronically excited $N_2(E)$ (mainly $N_2(A^3\Sigma)$ at 6.2 eV, and $N_2(B^3\Pi)$ at 7.4 eV), and a contribution of 8.5 % from the vibrationally excited $N_2(v)$ (mainly from the levels v=10-14 which are near the threshold energy for N_2 oxidation). The other Zeldovich reaction, **reaction 10**, is found on average to contribute ~18 % to NO formation. The remainder NO is derived from non-Zeldovich reactions, including the reaction of N and its electronically excited state $N(^2D)$ with $CO_2/CO_2(V_{a-d})$ (contributing for ~20 %), while three-body reactions of N and O atoms with $CO_2/CO_2(V_{a-d})$ account for ~11 %. In summary, the majority of NO formation is found to occur by a combination of the electronically and vibrationally enhanced Zeldovich reactions (**reaction 9** and **reaction 10**), with a total contribution of nearly 70%. This is beneficial, because the electronically and vibrationally excited levels lower the energy threshold of these reactions, thus contributing to energy-efficient NO_x formation. The Zeldovich reaction scheme for NO_x production, as predicted here, is a well-known reaction pathway for nitrogen oxidation. Indeed, this mechanism is consistent with our earlier works in both O_2/N_2 mixtures [36,75-78] and CO_2/N_2 mixtures [74], giving us confidence in the model's capability to describe the chemical mechanisms, in spite of the low NO_x levels predicted.

Finally, our model also provides information on other key plasma parameters, such as electron density and electron temperature. Averaged over the plasma region (i.e., 0-20 cm), they were found to be 3.3×10^{12} cm^{-3} and 0.51 eV, respectively. This is consistent with previous experimental reports on MW plasmas under similar conditions [35,79].

Utilisation scenarios

Future progress of plasma-based ISRU on Mars will need to capitalise on the promising metrics demonstrated here, but will also need to solve outstanding hurdles, by integrating any plasma conversion process with efficient gas separation technologies for a particular utilisation scenario [2]. Adsorption techniques (i.e., pressure or temperature swing adsorption) for both CO and O_2 separation from $O_2/CO/CO_2$ and CO/CO_2 mixtures are an important separation technology in a Martian ISRU context [80]. *Carbajo et al.* [81] recently investigated the use of zeolite materials for separation of a typical plasma produced $CO/O_2/CO_2$ mixture using pressure swing adsorption (PSA). The authors showed that existing commercial materials should perform well (i.e., give reasonably high purity ~96 %) under mild conditions (i.e., ~2 bar). The current energy cost of compression for MOXIE is about ~1-2 Wh/g CO_2 [14,69,82] (pressure range 0.34-1 bar), so a downstream PSA system to separate CO or O_2 would likely have an energy cost on this order (i.e., ~1-2 Wh/g CO, O_2). In our case the gas inlet flow rate is ~1100 g/h CO_2, so the energy costs for compression for a downstream PSA stage would likely be similar to the plasma conversion costs (i.e., per g O_2 or CO produced), yielding a total energy cost, including separation, in the order of ~0.04 kWh/g for O_2 production, or ~0.026 kWh/g for CO production, based on the promising metrics reported here. Hence, these combined costs could still fall significantly below MOXIE. However, this combination of plasma-based CO_2 splitting and PSA still needs to be tested in practice, to confirm these numbers, which are now only theoretical estimates. Furthermore, these separation methods do not account for the nitrogen fixation part. A notable downside of adsorption techniques like PSA is the difficulty of attaining very high purity (i.e., > 96 % O_2), which may be of concern for O_2 utilisation in life support. Several consecutive adsorption and regeneration cycles would be necessary to increase purity [83], leading to higher energy costs. However, given the estimates here, this could still be quite competitive with MOXIE. Further, the ambient low-pressure conditions on Mars could provide a 'free' pressure differential (i.e., the technique known as vacuum pressure swing adsorption (VPSA)) to further reduce this energy overhead. Indeed, a MW plasma can be sustained across a wide pressure range (i.e., from ambient Martian pressures to

above Earth ambient pressures) and deposits excess energy (not used in chemistry) as heat, providing a thermal energy source. This operational flexibility could be valuable for incorporation into any multi-stage adsorption configuration, where combinations of temperature swing adsorption (TSA), PSA and VPSA could provide a rapid separation process (e.g., ~10-100 s) [84] amenable to coupling with intermittent (solar) electricity.

Combinations of plasma and solid oxide electrolysis (SOXE), i.e., technology of MOXIE which decomposes/electrolyzes CO_2 and separates out the O_2 product [14,69,82], could also offer an intriguing prospect for production of highly purified O_2. *Pandiyan et al.* [85] recently interrogated the electrolysis of a CO_2 MW plasma-exhaust mixture consisting of CO, O_2 and CO_2. The authors showed that O_2 separation, in particular, can be achieved exclusively at low overpotentials (i.e., < 0.75 V) and reduced temperatures (i.e., ~650 °C); conditions where CO oxidation and CO_2 electrolysis (i.e., dissociation of CO_2) are not active. The authors reported a promising energy reduction of > 50 % for O_2 production (i.e., separation) using this combined plasma-SOXE approach, compared to a pure CO_2 SOXE O_2 production. Feeding the SOXE cell with a $CO/O_2/CO_2$ (plasma) mix rather than pure CO_2 is also found to benefit considerably the cells durability, with similarities to the methodology of partial recycling of exhaust CO used in MOXIE [14]. Notably, any plasma-SOXE hybrid technology operating at reduced temperatures (i.e., < 650 °C) would be much more flexible to powering by intermittent electricity sources and better exploit the operational flexibility of plasma conversion. MOXIE is currently limited in the number of thermal cycles, possibly due to material degradation [14,69], so it cannot be easily switched on and off. On-going research efforts into low-temperature SOXE materials [86] could also have a significant impact on any future hybrid designs reaching more flexible operating conditions.

Obtaining a useable form of fixed nitrogen for farming on Mars could largely depend on the availability of water (e.g., extracted from Martian clays or regolith [87]). Water reacts readily with NO_2, a process exploited in the original BE process where NO is first oxidised to NO_2 in a settling tank before hydrolysing it in a washing column to form a nitric acid solution. This could potentially solve the separation problem of the formed NO_x from the other gas components (CO, O_2 and unconverted CO_2 and N_2). Contemporary advances suggest that the energy cost and size of any adsorption stage could be significantly reduced, e.g., using modern NO_x absorbents such as BaO [88,89] in combination with temperature/pressure swing adsorption [47]. Nitric acid could be deployed directly for use in a hydroponic 'soil-less' farm, serving as a direct source of nitrates for plant growth [90]. Applying an acid solution directly to soils in an open environment could lead to relatively poor uptake by plants due to the liquid's volatility. Soil-based Martian farms, as on Earth, would therefore likely benefit from solid forms of nitrogen fertiliser. Combinations with urine is one possible pathway to form solid nitrogen fertiliser. Mixing nitric acid with urine reacts readily (i.e., exothermically) to form urea nitrate, a solid crystalline material which can be mixed into soils as a fertiliser. Further, the fermentation of urine can produce ammonia gas, aided by the urease enzyme. Bubbling ammonia through nitric acid will readily (i.e., exothermically) produce the solid ammonium nitrate. Indeed, ammonium nitrate is the most common form of nitrogen fertiliser used today on Earth for soil-based farming. Notably both urea nitrate and ammonium nitrate are also powerful explosives with potential utility for excavation activities by future settlers.

In summary, we emphasise that the promise of producing O_2 and CO, while fixing nitrogen on Mars using plasma technology combined with SOXE and/or adsorption methods is, at present, largely conceptual; however, we believe this approach holds much potential for Mars ISRU and we hope that this paper can inspire future research efforts.

CONCLUSIONS

We demonstrate the novel possibility of fixing N_2 on Mars, besides CO_2 conversion to CO and O_2, using the local Martian atmosphere. Microwave (MW) plasma conversion of the majority CO_2 fraction (~96 %) in the Martian atmosphere results in O atom formation, which enables oxidation of the small N_2 fraction (~ 2%), and thus results in fixation of ~7 % of the N_2 present in a simulant Martian atmosphere. Our MW plasma investigation shows promising O_2, CO and NO_x production rates of 47.0, 76.1 and 1.25 g/h at an energy cost of 0.021, 0.013 and 0.79 kWh/g. Using the current energy allocation of 1 kWh available to the Mars Oxygen In-situ Electrolysis (MOXIE) experiment on NASA's Perseverance rover, our MW plasma produces 47.0 g/h of O_2, which is almost 30 times higher than the current capabilities of MOXIE (1.6 g/h), and at 10 times lower energy cost (0.021 kWh/g vs 0.19 kWh/g). Plasma-based conversion, therefore, shows great potential as a future Martian ISRU technology.

The technology also has the key benefit of a rapid start-up time and is therefore highly flexible to the intermittent availability of Martian solar electricity (i.e., energy storage could be forgone). However, the energy costs reported only consider the plasma process, and do not yet account for the cost of gas compression and separation, for which the combination with SOEC would be very interesting, especially because the hot plasma exhaust gas could activate a SOEC for downstream product separation. We hope this paper can inspire future research in this direction. Indeed, an efficient gas separation technology downstream, in combination with our plasma technology, could generate the pure chemical streams for utilisation as fertiliser, life support and fuel for future robotic and human exploration of the red planet.

EXPERIMENTAL PROCEDURES

Resource availability

Lead contact

Further information and requests for resources and materials should be directed to and will be fulfilled by the lead contact, Seán Kelly (sean.kelly@uantwerpen.be).

Materials availability

This study did not generate new unique materials.

Data and code availability

Data from this study are available from the lead contact upon reasonable request.

Experimental setup

A schematic of our setup and an image of our MW plasma reactor in operation with a Martian simulant mixture consisting of 96 % CO_2, 2 % N_2 and 2 % Ar are shown in **figure 3 A** and **figure 3 B**. The power supply is composed of a collection of laterally diffused metal oxide semiconductor (LDMOS) power amplifiers, from which the output powers are combined in a mixer waveguide (WR340). This waveguide is connected via an isolator and an auto-tuner to a tapered waveguide section, including a 16 mm inner diameter quartz tube. The latter is mounted perpendicularly through a coupling hole (i.e., < 1/4 wavelength in diameter), where the plasma ignition takes place. An auto-tuner, impedance analyser and adjustable short are used to tune the electric field to optimal conditions for electrical breakdown, and to sustain a continuously powered plasma with minimum reflected power (<< 5 %). Tangential gas injection ports coupled with a helical insert allow a

swirl or vortex flow within the quartz discharge tube. Upon ignition, a surface wave sustained mode [91] is generated, with the plasma filament located at the tube centre (see **figure 3 B** and **figure 3 C**). This provides a key benefit by isolating the warm plasma (~2000-3000 K) from the quartz tube walls, allowing for elongated and stable plasma column formation along the tube lateral axis. Once initiated, the surface wave mode is stable across a wide pressure range from low pressures (~0.1 bar) to several bar.

Analysis of the NO_x species (i.e., NO and NO_2) and CO in the exhaust gas is performed using non-dispersive infra-red and ultra-violet (NDIR/UV) absorption spectrometry (Rosemount X-STREAM XEGP Continuous Gas Analyzer [92]), while O_2 is measured using a PyroScience GmbH [93] sensor based on an infra-red luminescent quenched absorption technique. All diagnostics were calibrated using pre-mixed calibration gases (Air Liquide) and cross-checked with gas chromatography (GC) using the compact-GC instrument from Interscience. This GC has two channels, each with a Thermal Conductivity Detector (TCD), using carboxen and molsieve columns (1010 PLOT and 5A, respectively) for O_2, N_2 and CO detection, and two RT Q-bond columns (3 m and 10 m length, respectively) for CO_2 detection [94].

The primary gas converted in our experiments is CO_2 (96 % of the Martian atmosphere), with oxidation of the small N_2 content (2 %). The argon fraction (2 %) is not converted due to its inertness. The key overall reactions for consideration are therefore:

$$CO_2 \rightarrow CO + 1/2\ O_2 \qquad \textit{(Reaction 1)}$$

$$O_2 + N_2 \rightarrow 2\ NO \qquad \textit{(Reaction 2)}$$

$$2\ O_2 + N_2 \rightarrow 2\ NO_2 \qquad \textit{(Reaction 3)}$$

In any gas conversion process, there is typically gas expansion or contraction due to changes in stoichiometry. In our experiments this results in an increase to the mass outflow. Indeed, given CO_2 is the primary component of the gas fraction, plasma conversion to CO and O_2 results in an expansion of the inlet flow, which depends on the degree of conversion. Notably the formation of NO_2 results in gas contraction, however, due to the relatively small fraction of N_2 and even smaller fraction of NO_2 formed compared to CO and O_2, this has negligible effect compared to expansion from CO_2 conversion. Strategies for measuring the gas mass outflow can include direct measurement or inference of the degree of expansion/contraction using dilution gases. In our case, given the dominance of CO_2 conversion, the degree of expansion can be inferred using the CO_2 conversion as:

$$\alpha = 1 + 0.5 * \eta_{CO_2}^{converted} \qquad (4)$$

$$\eta_{CO_2}^{converted} = \frac{\eta_{CO_2}^{OFF} - \alpha * \eta_{CO_2}^{ON}}{\eta_{CO_2}^{OFF}} \qquad (5)$$

Where α represents the gas expansion factor (i.e., $\alpha > 1$), $\eta_{CO_2}^{converted}$ is the fraction of CO_2 converted, $\eta_{CO_2}^{OFF}$ is

the fraction of CO_2 in the mixture when the plasma is off (i.e., 0.96 in our case) and $\eta_{CO_2}^{ON}$ is the measured CO_2 fraction when the plasma is ON. Rearranging **equations 4** and **5** we can solve them to find α based on the measured CO_2:

$$\alpha = \frac{1.5 * \eta_{CO_2}^{OFF}}{\eta_{CO_2}^{OFF} + 0.5 * \eta_{CO_2}^{ON}} \qquad (6)$$

Subsequently, when knowing α, we obtain the CO_2 conversion by **equation 5.** The CO, O_2 and NO_x production rates are calculated based on the percentage yield of each species measured in the exhaust and using the corresponding mass flow rate adjusted for the gas expansion. The individual production rates are then calculated for CO, O_2 and NO_x (NO +NO_2) as:

$$PR_{CO,O_2,NO_x}[g/h] = \frac{\eta_{CO,O_2,NO_x} * \mu_{CO,O_2,NO_x}[g/mol] * \alpha * f_{in}[L/min]}{22.4\,[L/mol]} * 60\,[min/h] \qquad (7)$$

where the production rate, PR [g/h], is determined by the inlet mass flow rate f_{in}[L/min] (standard litres per minute) for the Martian atmosphere simulant mix, consisting of 96 % CO_2, 2 % N_2 and 2% Ar. $\eta_{CO/O_2/NO_x}$ represents the fraction of species produced, directly measured in the plasma exhaust while μ_{CO,O_2,NO_x} [g/mol] is the molar mass of CO, O_2 or NO_x, and 22.4 [L/mol] is the molar volume of a gas under the corresponding standard conditions (i.e., standard temperature and pressure) for which our mass flow controllers are calibrated.

The energy cost for the production of CO, O_2 or NO_x is then obtained using:

$$EC_{CO,O_2,NO_x}\,[kWh/g] = \frac{Power\,[kW]}{PR_{CO,O_2,NO_x}\,[g/h]} \qquad (8)$$

where the Power [kW or kJ/s] is the absorbed MW power measured during steady state plasma operation.

Numerical modelling and chemistry

A quasi-1D chemical kinetics model is employed using the ZDPlasKin (Zero-Dimensional Plasma Kinetics) solver [95-97]. An overview of the simulation scheme is given in **figure 4** with full details of the equations employed found in our earlier work [36]. The time-evolution of the species densities, including electrons, and various charged and neutral species, is calculated by balance equations, considering the production and loss terms by chemical reactions. Dynamic changes in the gas velocity due to temperature and stoichiometric changes in the gas mixture are updated on each time step.

The power density $P[W/\mathrm{cm}^3]$ is derived from our experimental measurements of the absorbed power (i.e., forward minus reflected power) combined with determination of the plasma volume via camera imaging inside the tapered section of the waveguide (see **figure 3 B** and **figure 3 C**). A cylindrical shape is assumed for the plasma volume [98]. This is consistent with vortex-stabilised discharges, where the plasma is contained within the tube inner region, separated from the containment walls by a swirling or vortex flow boundary. The plasma elongates along the direction of the flow (i.e., along the axial extent of the reactor tube) forming a cylindrical shape in its steady state [34,98,99]. In order to account for the radial variation in power density from

the centre of the plasma filament to its edge, the light emission across the radial extent of the plasma filament at its ignition point inside the waveguide (as shown in **figure 3 C**) is used as a proxy for the plasma width. We therefore solve the quasi-1D model for two different radial sections, with a corresponding high power density of the plasma core and a relatively low power density to represent the plasma edge, as explained in our earlier paper [36]. For each of both quasi-1D models, we assume a triangular distribution of power density in the lateral extent of the plasma (i.e., along the direction of gas flow), in line with earlier modelling of power dissipation in surface wave sustained MW plasmas [58,100].

The reduced electric field, i.e., the ratio of electric field over gas number density, a key fundamental variable defining the plasma characteristics, is calculated from our measured specified power density (see **figure 4**). A Boltzmann solver (i.e., BOLSIG+) is utilised to simulate electron dynamics by linking the plasma conductivity (a function of the reduced electric field) to the electron mobility. Further to this, the gas temperature is solved in the model at each time step, based on gas heating due to elastic collisions of electrons with the gas molecules, the enthalpy contributions from the chemical reactions between all plasma species, heat losses to the walls and the dynamic heat capacity taking account of the gas mixture. The radially averaged gas temperature (which is assumed to have a parabolic profile) is calculated by considering the time-dependent gas thermal balance equation under isobaric conditions. Further details can be found in our earlier works [36,71,101,102].

The Martian air chemistry (i.e., $CO_2/N_2/Ar$) employed here is assembled from our earlier works, where details can be found [71,74,103]. 149 species are included in the model, i.e., the electrons, CO_2, Ar, N_2, O_2, CO, various N_xO_y molecules in ground state, along with various (vibrational and electronic) excited levels, various radicals, atoms and ions (see **Table 1**). These species react with each other in 973 electron impact reactions and 12,604 heavy particle reactions (i.e., between molecules in ground state or excited levels, radicals, atoms or ions). For the heavy particle reactions, the rate coefficients are adopted from our earlier works, whereas the rate coefficients for the electron impact reactions are calculated using the Boltzmann solver BOLSIG+ [97] built in ZDPlasKin.

Plasma-based conversion of relatively inert molecules, such as N_2 and CO_2, provides unique reaction pathways not available in purely thermal conversion. Especially in MW plasma, the electrons have the right energy (~ 1 eV) to cause excitation towards the lowest vibrational levels in $CO_2/N_2/O_2$, followed by further vibrational-vibrational (V-V) collisions, which enable a "ladder-climbing" process, gradually populating higher vibrational levels (denoted as e.g., $CO_2(V)$ and $N_2(V)$). Further significant populations of electronically excited species (e.g., $CO_2(E)$ and $N_2(E)$) can form inside the plasma region. Such species serve to lower the overall energy required for CO_2 dissociation (i.e., O_2 formation) and NO_x formation, as their higher energy levels help to overcome the activation barriers.

The underlying elementary reactions for NO_x production (see overall **reactions 2** and **3** above) in a plasma involve the atoms formed upon dissociation of the corresponding molecules, and proceed via the (electronically or vibrationally enhanced) Zeldovich mechanism [53,104,105] consisting of the following reactions:

$$O + N_2/N_2(E,V) \leftrightarrow N + NO \qquad \textit{(Reaction 9)}$$

$$N + O_2/O_2(E,V) \leftrightarrow O + NO \qquad \textit{(Reaction 10)}$$

The above reaction pair is typically rate-limited by **reaction 9,** given the energy requirement for overcoming the strong N_2 triple bond. Notably, the mechanism here can be significantly different from the purely thermal Zeldovich mechanism (i.e., involving only ground state N_2 and O_2) due to the presence of vibrationally or electronically excited N_2 and O_2 molecules, available in plasmas. The vibrationally or electronically excited N_2 molecules lower the dissociation threshold required to break the N_2 bond (~9.8 eV) through colliding with O atoms (i.e., **reaction 9**). The N atoms formed in **reaction 9** can then further react with both ground state and vibrationally/electronically excited O_2 molecules (**reaction 10**) to produce another NO. **Reaction 10** also produces an additional O atom, which can again react with ground state and vibrationally/electronically excited N_2 molecules (i.e., **reaction 9**), or oxidise NO to produce NO_2 (**reaction 11**):

$$NO + O \rightarrow NO_2 \qquad \textit{(Reaction 11)}$$

A similar oxidation pathway applies to CO_2. The overall **reaction 1** above includes the following elementary reactions, involving atomic oxygen:

$$CO_2(E,V) \rightarrow CO + O \qquad \textit{(Reaction 12)}$$

$$CO_2(E,V) + O \rightarrow CO + O_2 \qquad \textit{(Reaction 13)}$$

Direct dissociation processes in **reaction 12,** such as electron impact dissociation, have an energy threshold of 5.5 eV to overcome the (ground state) CO_2 bond energy, but the atomic oxygen produced in **reaction 12** can further react (i.e., **reaction 13**) with CO_2 (and its vibrationally or electronically excited states). This coupling lowers the threshold considerably (e.g., for ground state CO_2 this lowers the overall energy threshold to 2.9 eV [35]).

SUPPLEMENTAL INFORMATION

Document '**Supp_info.pdf**' is the main supplemental PDF.

ACKNOWLEDGEMENTS

We acknowledge financial support by an European Space Agency Open Science Innovation Platform study (Contract No. 4000137001/21/NL/GLC/ov), the European Marie Skłodowska-Curie Individual Fellowship "PENFIX" within Horizon 2020 (Grant No. 838181), the European Research Council (ERC) under the European Union's Horizon 2020 research and innovation program (grant agreement No 810182 – SCOPE ERC Synergy project), and the Excellence of Science FWO-FNRS project (FWO grant ID G0F9618n, EOS ID 30505023). CV was supported by FWO – PhD fellowship-aspirant, Grant 1184820N. The calculations were performed using the Turing HPC infrastructure at the CalcUA core facility of the Universiteit Antwerpen (UAntwerpen), a division of the Flemish Supercomputer Centre VSC, funded by the Hercules Foundation, the Flemish Government (department EWI) and the UAntwerpen. We thank Dr. Waldo Bongers and Dr. Floran Peeters of DIFFER for their help and advice in the initial phase of the project, Mr. Luc van 't dack, Dr. Karen Leyssens and Ing. Karel Venken for their adept technical assistance, Arn Van Hemelen for his work on the project during

his bachelor studies, Dr. Kevin van 't Veer and Dr. Josh Boothroyd for their very helpful discussions and assistance with the modelling. We thank Dr. Klaus Werner of PinkRF for discussions on solid-state MW technology and Dr. Pluton Pullumbi & Dr. Pascal Barbier of Air Liquide for discussions on gas separation technologies. Finally, we thank Dr. Brandon Buergler of ESA for discussions regarding solid oxide electrolysis technology.

AUTHOR CONTRIBUTIONS

S.K. conducted the experiments and modelling including data analysis; S.K., A.C and A.B. wrote the paper. C.V. conducted modelling and compiled the chemistry.

DECLARATION OF INTERESTS

The authors declare no competing interests.

REFERENCES

1. Foing, B.H. (2018). Reaction: Surviving on the Moon, Mars, and Asteroids. Chem *4*, 14-15. 10.1016/j.chempr.2017.12.020.
2. Sanders, G.B., Paz, A., Oryshchyn, L., Araghi, K., Muscatello, A., Linne, D.L., Kleinhenz, J.E., and Peters, T. Mars ISRU for Production of Mission Critical Consumables - Options, Recent Studies, and Current State of the Art. In AIAA SPACE 2015 Conference and Exposition. 10.2514/6.2015-4458.
3. Hepp, A.F., Palaszewski, B.A., Colozza, A.J., Landis, G.A., Jaworske, D.A., and Kulis, M.J. (2014). In-Situ Resource Utilization for Space Exploration: Resource Processing, Mission-Enabling Technologies, and Lessons for Sustainability on Earth and Beyond. In 12th International Energy Conversion Engineering Conference, (American Institute of Aeronautics and Astronautics). doi:10.2514/6.2014-3761.
4. Schlüter, L., and Cowley, A. (2020). Review of techniques for In-Situ oxygen extraction on the moon. Planetary and Space Science *181*, 104753. 10.1016/j.pss.2019.104753.
5. Starr, S.O., and Muscatello, A.C. (2020). Mars in situ resource utilization: a review. Planetary and Space Science *182*, 104824. 10.1016/j.pss.2019.104824.
6. Casini, A.E.M., Maggiore, P., Viola, N., Basso, V., Ferrino, M., Hoffman, J.A., and Cowley, A. (2018). Analysis of a Moon outpost for Mars enabling technologies through a Virtual Reality environment. Acta Astronautica *143*, 353-361. j.actaastro.2017.11.023.
7. Drake, B.G., Hoffman, S.J., and Beaty, D.W. (2010). Human exploration of Mars, Design Reference Architecture 5.0. 6-13 March 2010. pp. 1-24.
8. Sridhar, K.R., and Vaniman, B.T. (1997). Oxygen production on Mars using solid oxide electrolysis. Solid State Ionics *93*, 321-328. https://doi.org/10.1016/S0167-2738(96)00513-9.
9. European Space Agency (ESA) Ariane 5G payload average cost Kg/$ for 24 missions. (2021). Aerospace Security https://aerospace.csis.org/data/space-launch-to-low-earth-orbit-how-much-does-it-cost/.
10. Rapp, D. (2015). Human Missions to Mars: Enabling Technologies for Exploring the Red Planet (Springer Cham). https://doi.org/10.1007/978-3-319-22249-3.
11. European Space Agency (ESA) Exomars programme, https://exploration.esa.int/s/wKQB3q8.
12. Schulze-Makuch, D., Heller, R., and Guinan, E. (2020). In Search for a Planet Better than Earth: Top Contenders for a Superhabitable World. Astrobiology *20*, 1394-1404. 10.1089/ast.2019.2161.
13. National Aeronautcal Spance Agency (NASA) , Mars Oxygen In-Situ Resource Utilization Experiment (MOXIE), https://mars.nasa.gov/mars2020/spacecraft/instruments/moxie/. (2020).
14. Hecht, M., Hoffman, J., Rapp, D., McClean, J., SooHoo, J., Schaefer, R., Aboobaker, A., Mellstrom,

J., Hartvigsen, J., Meyen, F., et al. (2021). Mars Oxygen ISRU Experiment (MOXIE). Space Science Reviews *217*, 9. 10.1007/s11214-020-00782-8.
15. MIT(Massachusetts Institute of Technology), p.r. (2021). Aboard NASA's Perseverance rover, MOXIE creates oxygen on Mars, https://news.mit.edu/2021/aboard-nasa-perseverance-mars-rover-moxie-creates-oxygen-0421.
16. Loer, Stephan A., Scheeren, Thomas W.L., and Tarnow, J. (1997). How Much Oxygen Does the Human Lung Consume? Anesthesiology *86*, 532-537. 10.1097/00000542-199703000-00004.
17. Nelson, M., and Dempster, W.F. (1995). Living in space: results from Biosphere 2's initial closure, an early testbed for closed ecological systems on Mars. Life Support Biosph Sci *2*, 81-102.
18. Linne, D. Carbon monoxide and oxygen combustion experiments - A demonstration of Mars in situ propellants. In 27th Joint Propulsion Conference. 10.2514/6.1991-2443.
19. Ash, R.L., Dowler, W.L., and Varsi, G. (1978). Feasibility of rocket propellant production on Mars. Acta Astronautica *5*, 705-724. 10.1016/0094-5765(78)90049-8.
20. Bogaerts, A., and Neyts, E.C. (2018). Plasma Technology: An Emerging Technology for Energy Storage. ACS Energy Letters *3*, 1013-1027. 10.1021/acsenergylett.8b00184.
21. Snoeckx, R., and Bogaerts, A. (2017). Plasma technology - a novel solution for CO2 conversion? Chem Soc Rev *46*, 5805-5863. 10.1039/c6cs00066e.
22. Haberle, R.M. (2017). The Atmosphere and Climate of Mars (Cambridge University Press). DOI:10.1017/9781139060172.
23. B. Franz, H., G. Trainer, M., H. Wong, M., L.K. Manning, H., C. Stern, J., R. Mahaffy, P., K. Atreya, S., Benna, M., G. Conrad, P., N. Harpold, D., et al. (2014). Analytical techniques for retrieval of atmospheric composition with the quadrupole mass spectrometer of the Sample Analysis at Mars instrument suite on Mars Science Laboratory. Planetary and Space Science *96*, 99-113. 10.1016/j.pss.2014.03.005.
24. Wu, D., Outlaw, R.A., and Ash, R.L. (1996). Extraction of oxygen from CO2 using glow‐discharge and permeation techniques. Journal of Vacuum Science & Technology A *14*, 408-414. 10.1116/1.580098.
25. Gruenwald, J. (2014). Human outposts on Mars: engineering and scientific lessons learned from history. CEAS Space Journal *6*, 73-77. 10.1007/s12567-014-0059-8.
26. Gruenwald, J. (2016). A hybrid plasma technology life support system for the generation of oxygen on Mars: Considerations on materials and geometry. Acta Astronautica *123*, 188-191. 10.1016/j.actaastro.2016.03.021.
27. Guerra, V., Silva, T., Ogloblina, P., Grofulović, M., Terraz, L., Silva, M.L.d., Pintassilgo, C.D., Alves, L.L., and Guaitella, O. (2017). The case for in situ resource utilisation for oxygen production on Mars by non-equilibrium plasmas. Plasma Sources Science and Technology *26*, 11LT01. 10.1088/1361-6595/aa8dcc.
28. Ogloblina, P., Morillo-Candas, A.S., Silva, A.F.S.d., Silva, T.P., Tejero-del-Caz, A., Alves, L., Guaitella, O., and Guerra, V. (2021). Mars in situ oxygen and propellant production by non-equilibrium plasmas. Plasma Sources Science and Technology.
29. Premathilake, D., Outlaw, R.A., Quinlan, R.A., and Byvik, C.E. (2019). Oxygen Generation by Carbon Dioxide Glow Discharge and Separation by Permeation Through Ultrathin Silver Membranes. Earth and Space Science *6*, 557-564. https://doi.org/10.1029/2018EA000521.
30. Moses, R.W., Kuhl, C.A., and Templeton, J. (2005). Plasma Assisted ISRU at Mars. held in Moscow.
31. Richard R. Wheeler, J., Neal M. Hadley, Spencer R. Wambolt, John T. Holtsnider, Ross Dewberry and Laurel J. Karr (2015). Plasma Extraction of Oxygen from Martian Atmosphere (PEOMA). (https://ttu-ir.tdl.org/bitstream/handle/2346/64474/ICES_2015_submission_203.pdf?sequence=1).
32. Fridman, A. (2008). Plasma Chemistry (Cambridge University Press). 10.1017/cbo9780511546075.

33. Bogaerts, A., and Centi, G. (2020). Plasma Technology for CO2 Conversion: A Personal Perspective on Prospects and Gaps. Frontiers in Energy Research *8*. 10.3389/fenrg.2020.00111.
34. Wolf, A.J., Righart, T.W.H., Peeters, F.J.J., Groen, P.W.C., van de Sanden, M.C.M., and Bongers, W.A. (2019). Characterization of CO2 microwave plasma based on the phenomenon of skin-depth-limited contraction. Plasma Sources Science and Technology *28*, 115022. 10.1088/1361-6595/ab4e61.
35. Bongers, W., Bouwmeester, H., Wolf, B., Peeters, F., Welzel, S., van den Bekerom, D., den Harder, N., Goede, A., Graswinckel, M., Groen, P.W., et al. (2017). Plasma-driven dissociation of CO2 for fuel synthesis. Plasma Processes and Polymers *14*, 1600126. 10.1002/ppap.201600126.
36. Kelly, S., and Bogaerts, A. (2021). Nitrogen fixation in an electrode-free microwave plasma. Joule *5*, 3006-3030. 10.1016/j.joule.2021.09.009.
37. Winter, L.R., and Chen, J.G. (2021). N2 Fixation by Plasma-Activated Processes. Joule *5*, 300-315. 10.1016/j.joule.2020.11.009.
38. Wamelink, G.W.W., Frissel, J.Y., Krijnen, W.H.J., Verwoert, M.R., and Goedhart, P.W. (2014). Can Plants Grow on Mars and the Moon: A Growth Experiment on Mars and Moon Soil Simulants. PLoS ONE *9*, e103138. 10.1371/journal.pone.0103138.
39. Eichler, A., Hadland, N., Pickett, D., Masaitis, D., Handy, D., Perez, A., Batcheldor, D., Wheeler, B., and Palmer, A. (2021). Challenging the agricultural viability of martian regolith simulants. Icarus *354*, 114022. 10.1016/j.icarus.2020.114022.
40. Fackrell, L.E., Schroeder, P.A., Thompson, A., Stockstill-Cahill, K., and Hibbitts, C.A. (2021). Development of martian regolith and bedrock simulants: Potential and limitations of martian regolith as an in-situ resource. Icarus *354*, 114055. 10.1016/j.icarus.2020.114055.
41. Wamelink, G.W.W., Frissel, J.Y., Krijnen, W.H.J., and Verwoert, M.R. (2019). Crop growth and viability of seeds on Mars and Moon soil simulants. Open Agriculture *4*, 509-516. doi:10.1515/opag-2019-0051.
42. Certini, G., Karunatillake, S., Zhao, Y.-Y.S., Meslin, P.-Y., Cousin, A., Hood, D.R., and Scalenghe, R. (2020). Disambiguating the soils of Mars. Planetary and Space Science *186*, 104922. 10.1016/j.pss.2020.104922.
43. Mancinelli, R.L., and Banin, A. (2003). Where is the nitrogen on Mars? International Journal of Astrobiology *2*, 217-225. 10.1017/S1473550403001599.
44. Silverstone, S.E. (1997). Food production and nutrition for the crew during the first 2-year closure of Biosphere 2. Life Support Biosph Sci *4*, 167-178.
45. Lim, S., Rood, C., and Hassanalian, M. (2020). Examination of Explosives in Martian Atmospheric Conditions. In AIAA Propulsion and Energy 2020 Forum, (American Institute of Aeronautics and Astronautics). 10.2514/6.2020-3652.
46. Dick, R.D., Fourney, W.L., Goodings, D.J., Lin, C.-P., and Bernold, L.E. (1992). Use of explosives on the moon. Journal of Aerospace Engineering *5*, 59-69.
47. Rouwenhorst, K., Jardali, F., Bogaerts, A., and Lefferts, L. (2021). From the Birkeland-Eyde process towards energy-efficient plasma-based NOx synthesis: A techno-economic analysis. Energy & Environmental Science *14*, 2520-2534. 10.1039/d0ee03763j.
48. Patil, B.S., Wang, Q., Hessel, V., and Lang, J. (2015). Plasma N2-fixation: 1900–2014. Catalysis Today *256*, 49-66. 10.1016/j.cattod.2015.05.005.
49. Chen Jingguang, G., Crooks Richard, M., Seefeldt Lance, C., Bren Kara, L., Bullock, R.M., Darensbourg Marcetta, Y., Holland Patrick, L., Hoffman, B., Janik Michael, J., Jones Anne, K., et al. (2018). Beyond fossil fuel–driven nitrogen transformations. Science *360*, eaar6611. 10.1126/science.aar6611.
50. Birkeland, K. (1906). On the oxidation of atmospheric nitrogen in electric arcs. Transactions of the Faraday Society *2*, 98-116. 10.1039/TF9060200098.

51. Cherkasov, N., Ibhadon, A.O., and Fitzpatrick, P. (2015). A review of the existing and alternative methods for greener nitrogen fixation. Chemical Engineering and Processing: Process Intensification *90*, 24-33. 10.1016/j.cep.2015.02.004.
52. Eyde, H.S. (1909). The Manufacture of nitrates from atmosphere by the electric arc - Birkeland-Eyde Process. Journal of the Royal Society of Arts *57*, 568-576.
53. Wang, W., Patil, B., Heijkers, S., Hessel, V., and Bogaerts, A. (2017). Nitrogen Fixation by Gliding Arc Plasma: Better Insight by Chemical Kinetics Modelling. ChemSusChem *10*, 2145-2157. 10.1002/cssc.201700095.
54. Knox, J. (1914). The Fixation of Atmospheric Nitrogen (Gurney & Jackson).
55. Horikoshi, S., and Serpone, N. (2020). RF Power Semiconductor Generator Application in Heating and Energy Utilization (Springer Singapore).
56. Werner, K.T., S. (2012). RF Driven Plasma Lighting: The Next Revolution in Light Sources. Microwave Journal.
57. (HHF), H.H.-T.G. (2020). Jets PC-Series plasma reactors. https://hhft.de/microwave-plasma.
58. Berthelot, A., and Bogaerts, A. (2017). Modeling of CO2 Splitting in a Microwave Plasma: How to Improve the Conversion and Energy Efficiency. The Journal of Physical Chemistry C *121*, 8236-8251. 10.1021/acs.jpcc.6b12840.
59. Whittlesey, A.C., and Lumsden, J.M. (1981). Electric Welding Hazard to Spacecraft Electronics. 1981 IEEE International Symposium on Electromagnetic Compatibility, 1-5.
60. Bodeau, M. (2019). Mitigating Potential Hazards of TIG Welding on Spacecraft. IEEE Transactions on Electromagnetic Compatibility *61*, 90-99.
61. Werner, K. (2020). Pink RF, RF energy solutions https://www.pinkrf.com/products/power-amplifiers/.
62. Bai, W., Feng, J., Luo, C., Zhang, P., Wang, H., Yang, Y., Zhao, Y., and Fan, H. (2021). A comprehensive review on oxygen transport membranes: Development history, current status, and future directions. International Journal of Hydrogen Energy *46*, 36257-36290. https://doi.org/10.1016/j.ijhydene.2021.08.177.
63. Liu, J., Ma, K., Ciais, P., and Polasky, S. (2016). Reducing human nitrogen use for food production. Scientific Reports *6*, 30104. 10.1038/srep30104.
64. Zhang, X. (2017). A plan for efficient use of nitrogen fertilizers. Nature *543*, 322-323. 10.1038/543322a.
65. Rockström, J., Steffen, W., Noone, K., Persson, Å., Chapin, F.S., Lambin, E.F., Lenton, T.M., Scheffer, M., Folke, C., Schellnhuber, H.J., et al. (2009). A safe operating space for humanity. Nature *461*, 472-475. 10.1038/461472a.
66. British Petroleum Company. BP statistical review of world energy. https://www.bp.com/en/global/corporate/energy-economics/statistical-review-of-world-energy.html. (2021).
67. Ramírez, C.A., and Worrell, E. (2006). Feeding fossil fuels to the soil: An analysis of energy embedded and technological learning in the fertilizer industry. Resources, Conservation and Recycling *46*, 75-93. https://doi.org/10.1016/j.resconrec.2005.06.004.
68. Jouhara, H., Khordehgah, N., Almahmoud, S., Delpech, B., Chauhan, A., and Tassou, S.A. (2018). Waste heat recovery technologies and applications. Thermal Science and Engineering Progress *6*, 268-289. https://doi.org/10.1016/j.tsep.2018.04.017.
69. Meyen, F.E., Hecht, M.H., and Hoffman, J.A. (2016). Thermodynamic model of Mars Oxygen ISRU Experiment (MOXIE). Acta Astronautica *129*, 82-87. https://doi.org/10.1016/j.actaastro.2016.06.005.
70. Kozák, T., and Bogaerts, A. (2014). Evaluation of the energy efficiency of CO2conversion in microwave discharges using a reaction kinetics model. Plasma Sources Science and Technology *24*,

015024. 10.1088/0963-0252/24/1/015024.
71. Heijkers, S., Snoeckx, R., Kozák, T., Silva, T., Godfroid, T., Britun, N., Snyders, R., and Bogaerts, A. (2015). CO2 Conversion in a Microwave Plasma Reactor in the Presence of N2: Elucidating the Role of Vibrational Levels. The Journal of Physical Chemistry C *119*, 12815-12828. 10.1021/acs.jpcc.5b01466.
72. Vermeiren, V., and Bogaerts, A. (2019). Improving the Energy Efficiency of CO2 Conversion in Nonequilibrium Plasmas through Pulsing. The Journal of Physical Chemistry C *123*, 17650-17665. 10.1021/acs.jpcc.9b02362.
73. Vermeiren, V., and Bogaerts, A. (2020). Plasma-Based CO2 Conversion: To Quench or Not to Quench? The Journal of Physical Chemistry C *124*, 18401-18415. 10.1021/acs.jpcc.0c04257.
74. Ramakers, M., Heijkers, S., Tytgat, T., Lenaerts, S., and Bogaerts, A. (2019). Combining CO2 conversion and N2 fixation in a gliding arc plasmatron. Journal of CO2 Utilization *33*, 121-130. https://doi.org/10.1016/j.jcou.2019.05.015.
75. Jardali, F., Van Alphen, S., Creel, J., Ahmadi Eshtehardi, H., Axelsson, M., Ingels, R., Snyders, R., and Bogaerts, A. (2021). NOx production in a rotating gliding arc plasma: potential avenue for sustainable nitrogen fixation. Green Chemistry *23*, 1748-1757. 10.1039/d0gc03521a.
76. Van Alphen, S., Jardali, F., Creel, J., Trenchev, G., Snyders, R., and Bogaerts, A. (2021). Sustainable gas conversion by gliding arc plasmas: a new modelling approach for reactor design improvement. Sustainable Energy & Fuels *5*, 1786-1800. 10.1039/D0SE01782E.
77. Vervloessem, E., Aghaei, M., Jardali, F., Hafezkhiabani, N., and Bogaerts, A. (2020). Plasma-Based N2 Fixation into NOx: Insights from Modeling toward Optimum Yields and Energy Costs in a Gliding Arc Plasmatron. ACS Sustainable Chemistry & Engineering *8*, 9711-9720. 10.1021/acssuschemeng.0c01815.
78. Van Alphen, S., Ahmadi Eshtehardi, H., O'Modhrain, C., Bogaerts, J., Van Poyer, H., Creel, J., Delplancke, M.-P., Snyders, R., and Bogaerts, A. (2022). Effusion nozzle for energy-efficient NOx production in a rotating gliding arc plasma reactor. Chemical Engineering Journal *443*, 136529. https://doi.org/10.1016/j.cej.2022.136529.
79. van den Bekerom, D.C.M., Linares, J.M.P., Verreycken, T., van Veldhuizen, E.M., Nijdam, S., Berden, G., Bongers, W.A., van de Sanden, M.C.M., and van Rooij, G.J. (2019). The importance of thermal dissociation in CO2 microwave discharges investigated by power pulsing and rotational Raman scattering. Plasma Sources Science and Technology *28*, 055015. 10.1088/1361-6595/aaf519.
80. Walton, K., and LeVan, M. (2004). Separation of Carbon Monoxide and Carbon Dioxide for Mars ISRU, https://ntrs.nasa.gov/api/citations/20010024956/downloads/20010024956.pdf. 09/01/2004.
81. Perez-Carbajo, J., Matito-Martos, I., Balestra, S.R.G., Tsampas, M.N., van de Sanden, M.C.M., Delgado, J.A., Águeda, V.I., Merkling, P.J., and Calero, S. (2018). Zeolites for CO2–CO–O2 Separation to Obtain CO2-Neutral Fuels. ACS Applied Materials & Interfaces *10*, 20512-20520. 10.1021/acsami.8b04507.
82. Hinterman, E., and Hoffman, J.A. (2020). Simulating oxygen production on Mars for the Mars Oxygen In-Situ Resource Utilization Experiment. Acta Astronautica *170*, 678-685. https://doi.org/10.1016/j.actaastro.2020.02.043.
83. Luna-Triguero, A., Vicent-Luna, J.M., Jansman, M.J., Zafeiropoulos, G., Tsampas, M.N., van de Sanden, M.C.M., Akse, H.N., and Calero, S. (2021). Enhancing separation efficiency in European syngas industry by using zeolites. Catalysis Today *362*, 113-121. https://doi.org/10.1016/j.cattod.2020.03.061.
84. Hedin, N., Andersson, L., Bergström, L., and Yan, J. (2013). Adsorbents for the post-combustion capture of CO2 using rapid temperature swing or vacuum swing adsorption. Applied Energy *104*, 418-433. https://doi.org/10.1016/j.apenergy.2012.11.034.
85. Pandiyan, A., Kyriakou, V., Neagu, D., Welzel, S., Goede, A., van de Sanden, M.C.M., and

Tsampas, M.N. (2022). CO2 conversion via coupled plasma-electrolysis process. Journal of CO2 Utilization *57*, 101904. https://doi.org/10.1016/j.jcou.2022.101904.
86. Wachsman, E.D., and Lee, K.T. (2011). Lowering the temperature of solid oxide fuel cells. Science *334*, 935-939. 10.1126/science.1204090.
87. Abbud-Madrid, A., D.W. Beaty, D. Boucher, B. Bussey, R. Davis, L. Gertsch, L.E. Hays, J. Kleinhenz, M.A. Meyer, M., and Moats, R.P.M., A. Paz, N. Suzuki, P. van Susante, C. Whetsel, E.A. Zbinden (2016). Report of the Mars Water In-Situ Resource Utilization (ISRU) Planning (M-WIP) Study, http://mepag.nasa.gov/reports/Mars_Water_ISRU_Study.pptx. California Institute of Technology.
88. Schmitz, P.J., and Baird, R.J. (2002). NO and NO2 Adsorption on Barium Oxide: Model Study of the Trapping Stage of NOx Conversion via Lean NOx Traps. The Journal of Physical Chemistry B *106*, 4172-4180. 10.1021/jp0133992.
89. Fridell, E., Skoglundh, M., Westerberg, B., Johansson, S., and Smedler, G. (1999). NOxStorage in Barium-Containing Catalysts. Journal of Catalysis *183*, 196-209. https://doi.org/10.1006/jcat.1999.2415.
90. Cannon, K.M., and Britt, D.T. (2019). Feeding One Million People on Mars. New Space *7*, 245-254. 10.1089/space.2019.0018.
91. Moisan, M., and Pelletier, J. (2006). Physics of collisional plasmas. Application to high frequency discharges; Physique des plasmas collisionnels. Application aux decharges haute frequence (Springer). https://link.springer.com/content/pdf/bfm%3A978-94-007-4558-2%2F1.pdf.
92. Emerson Rosemount™ X-STREAM X2GP Continuous Gas Analyzer, https://www.emerson.com/en-us/catalog/rosemount-x-stream-x2gp-continuous-gas-analyzer. (2020).
93. PyroScience GmbH Firesting O2 sensor, https://www.pyroscience.com/en/. (2021).
94. Girard-Sahun, F., Biondo, O., Trenchev, G., van Rooij, G., and Bogaerts, A. (2022). Carbon bed post-plasma to enhance the CO2 conversion and remove O2 from the product stream. Chemical Engineering Journal *442*, 136268. https://doi.org/10.1016/j.cej.2022.136268.
95. Pancheshnyi, S., Eismann, B., Hagelaar, G.J.M., and Pitchford, L.C. (2008). Computer code ZDPlasKin. University of Toulouse, LAPLACE, CNRS-UPS-INP, Toulouse, France. www.zdplaskin.laplace.univ-tlse.fr
96. Thompson, G.D.B.a.S. (2013). DVODE solver - ordinary differential equation (ode) solver - a Fortran 90 version of the well-known VODE ode solver by Brown, Byrne, and Hindmarsh, http://www.radford.edu/thompson/vodef90web.html.
97. Hagelaar, G.J.M., and Pitchford, L.C. (2005). Solving the Boltzmann equation to obtain electron transport coefficients and rate coefficients for fluid models. Plasma Sources Science and Technology *14*, 722-733. 10.1088/0963-0252/14/4/011.
98. Van Alphen, S., Vermeiren, V., Butterworth, T., van den Bekerom, D.C.M., van Rooij, G.J., and Bogaerts, A. (2019). Power Pulsing To Maximize Vibrational Excitation Efficiency in N2 Microwave Plasma: A Combined Experimental and Computational Study. The Journal of Physical Chemistry C *124*, 1765-1779. 10.1021/acs.jpcc.9b06053.
99. Wolf, A.J., Righart, T.W.H., Peeters, F.J.J., Bongers, W.A., and van de Sanden, M.C.M. (2020). Implications of thermo-chemical instability on the contracted modes in CO2 microwave plasmas. Plasma Sources Science and Technology *29*, 025005. 10.1088/1361-6595/ab5eca.
100. Schlüter, H., and Shivarova, A. (2007). Travelling-wave-sustained discharges. Physics Reports *443*, 121-255.
101. Kelly, S., van de Steeg, A., Hughes, A., van Rooij, G., and Bogaerts, A. (2021). Thermal instability and volume contraction in a pulsed microwave N2 plasma at sub-atmospheric pressure. Plasma Sources Science and Technology *30*, 055005. 10.1088/1361-6595/abf1d6.
102. Snoeckx, R., Heijkers, S., Van Wesenbeeck, K., Lenaerts, S., and Bogaerts, A. (2016).

CO2conversion in a dielectric barrier discharge plasma: N2in the mix as a helping hand or problematic impurity? Energy & Environmental Science *9*, 999-1011. 10.1039/c5ee03304g.

103. Van Gaens, W., and Bogaerts, A. (2013). Kinetic modelling for an atmospheric pressure argon plasma jet in humid air. Journal of Physics D: Applied Physics *46*, 275201. 10.1088/0022-3727/46/27/275201.
104. Patil, B.S., Rovira Palau, J., Hessel, V., Lang, J., and Wang, Q. (2015). Plasma Nitrogen Oxides Synthesis in a Milli-Scale Gliding Arc Reactor: Investigating the Electrical and Process Parameters. Plasma Chemistry and Plasma Processing *36*, 241-257. 10.1007/s11090-015-9671-4.
105. Rashid Alievich, S. (2014). Selected Works of Yakov Borisovich Zeldovich, Volume I. In 26. Oxidation of Nitrogen in Combustion and Explosions, S. Rashid Alievich, ed. (Princeton University Press), pp. 404-410. doi:10.1515/9781400862979.404.

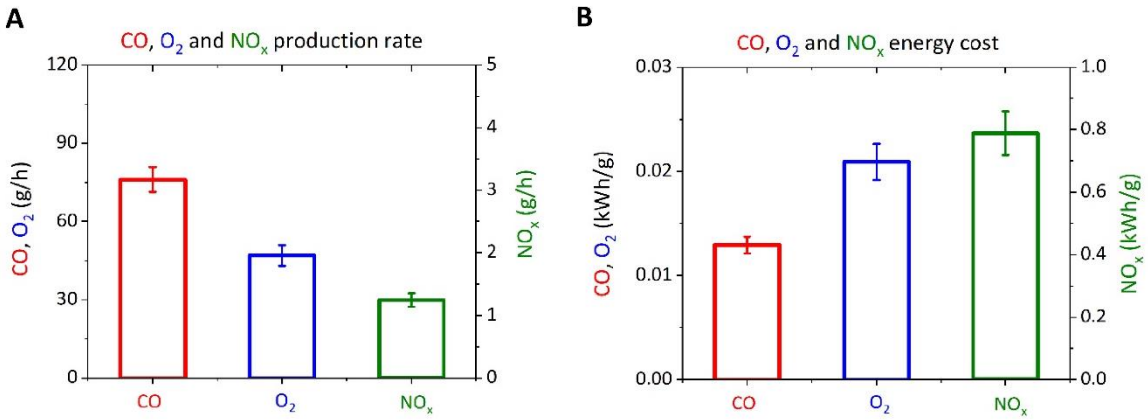

Figure 1: **A:** Absolute production rates (g/h) of CO, O_2 and NO_x; **B:** equivalent energy cost (kWh/g), in a MW plasma using a Martian simulant mixture of $CO_2/N_2/Ar$ (96/2/2 %) at 10 L/min flow rate, 0.34 bar pressure and 1 kW absorbed power. Note the NO_x data is indicated on the right-hand y-axes.

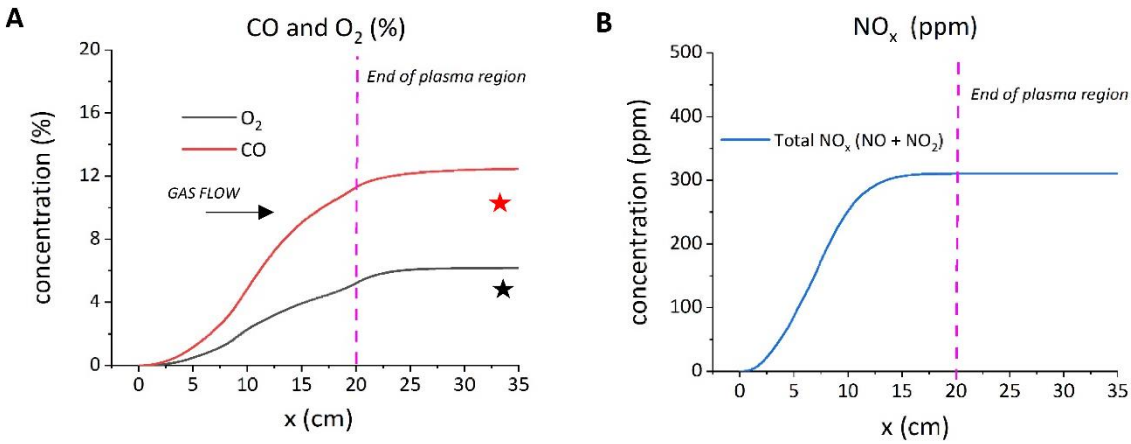

Figure 2: Calculated CO, O_2 (**figure 2 A**) and NO_x (**figure 2 B**) product concentrations as a function of position in and after the MW plasma, using a Martian simulant mixture of $CO_2/N_2/Ar$ (96/2/2% at 10 L/min flow rate, 0.34 bar pressure and 1 kW absorbed power). The measured CO and O_2 concentrations (downstream, hence after the plasma) are indicated with stars in **figure 2 A,** for comparison. The measured NO_x concentration is not added in **figure 2 B,** because there is still quite large discrepancy with the calculated value (see text). Note: the direction of gas flow through the plasma is along the positive x direction as indicated in the figure.

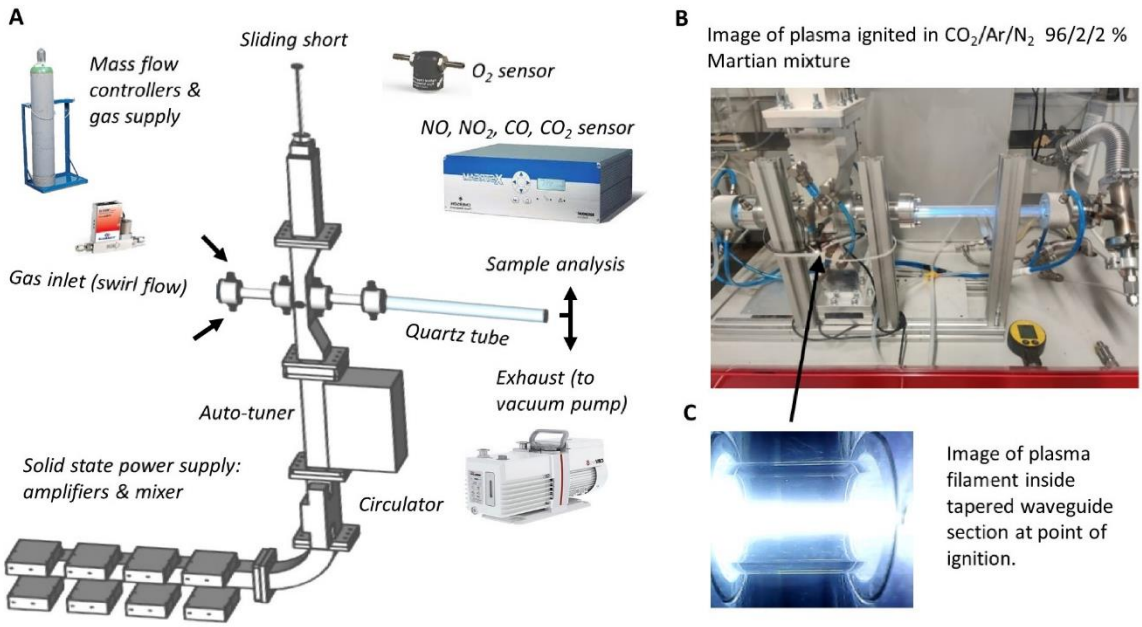

Figure 3: **A**: Illustration of our MW reactor consisting of a solid-state MW power supply, circulator, auto-tuner and tapered waveguide section terminated by a sliding short. The plasma is ignited inside a quartz tube where a swirling flow is injected. Sample analysis of the exhaust gas is carried out using an NDIR and a luminescence O_2 sensor. **B**: Photo of the reactor in operation with a Martian simulant atmosphere at 0.34 bar pressure and 1 kW power. Ignition takes place in a tapered section of a 2.45 GHz WR340 waveguide where a plasma is suspended at the centre of the tube. **C**: In-waveguide photo of the plasma; camera viewpoint is looking towards the quartz tube inside the waveguide, as indicated by the arrow.

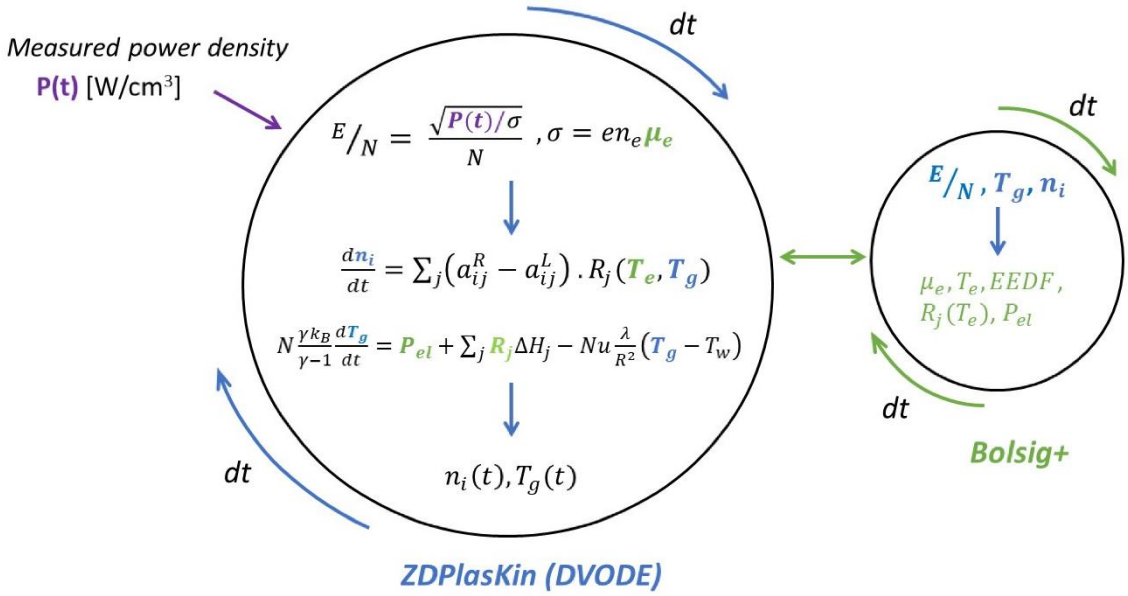

Figure 4: Overview of the numerical solution scheme for the quasi-1D model employing ZDPlasKin, which incorporates the DVODE code for ODE integration and BOLSIG+ to solve the Boltzmann equation at each time step. An experimentally determined power density [W/cm³] is coupled externally to enable solution via the reduced electric field E/N.

Table 1: Species included in our quasi-1D model for a $CO_2/N_2/Ar$ mixture.

Neutral	Excited	Charged
CO_2, CO, C_2O, C, C_2, CN, ONCN, NCO, NCN, C_2N, C_2N_2	$CO_2(V_a,V_b,V_c,V_d)$, $CO_2(V_1$-$V_{21})$, $CO_2(E_1)$, $CO(V_1$-$V_{10})$, $CO(E_1$-$E_4)$	CO_2^+, CO_4^+, CO^+, $C_2O_2^+$, $C_2O_3^+$, $C_2O_4^+$, C_2^+, C^+, CO_3^-, CO_4^-
O_2, O, O_3	$O_2(V_1$–$V_{15})$, $O_2(A_1\Delta)$, $O_2(A_3C_3C_1)$ §, $O_2(B_1\Sigma)$, O(1D), O(1S)	e, O^+, O^-, O_2^-, O_2^+, O_4^-, O_4^+, O_3^-
N_2, N, NO_2, NO, N_2O, N_2O_3, N_2O_4, N_2O_5	$N_2(V_1$–$V_{21})$, $N_2(^2D)$, $N_2(^3P)$, $N_2(A_1\Sigma)$, $N_2(A_3\Sigma)$, $N_2(B_3\Pi)$, $N_2(C_3\Pi)$	N_2^+, N_3^+, N_4^+, N^+, NO_2^+, NO_2^-, N_2O^-, N_2O^+, NO^+, NO^-, NO_3^-
Ar	$Ar(^4S)$, $Ar(^4P)$, $Ar_2(E)$ §§, $Ar(^4S^3[P_0])$, $Ar(^4S^3[P_1])$, $Ar(^4S^3[P_2])$, $Ar(^4S^1[P_1])$,	Ar^+, Ar_2^+

§: $O_2(A_3C_3C_1)$ is a combination of three electronically excited states $O_2(A^3\Sigma)$, $O_2(C^3\Delta)$ and $O_2(c^1\Sigma)$ with a threshold energy of 4.5 eV.

§§: $Ar_2(E)$ is a combination of the excited states $Ar_2(^1\Sigma)$ and $Ar_2(^3\Sigma)$ of the Ar_2 dimer.

For details about the notations of the other excited levels, see our earlier work [71,74,103].